
Check for updates

sample in the
can be rapidly increased up to 800 mbar
316L and the rou_316L samples were measured in additional measurements at 400°C and 500°C at four pressure steps (25 mbar, 100 mbar, 400 mbar, 800 mbar).

3. Data analysis

The permeation flux J_P through the sample dependents on the solubility and the diffusion coefficient of deuterium in the sample, and on surface processes, like dissociation of the deuterium molecule, absorption and desorption. In the diffusion-limited case, in which surface processes are quick and therefore negligible with respect to limiting the permeation process, the permeation flux can be expressed by [5,6]

$$J_P = \frac{P_0\sqrt{p}}{d} e^{\frac{-E_P}{RT}} \quad (1)$$

wherein d is the thickness of the sample, R is the ideal gas constant and T the temperature. The permeation constant P_0 is defined by $P_0 = D_0 K_0$ with the diffusion constant D_0 and the solubility constant K_0. The permeation activation energy E_P is defined by $E_P = E_D + \Delta H$ with the diffusion activation energy E_D and the standard enthalpy of dissolution ΔH. By measuring the deuterium permeation through the samples as a function of the pressure and the temperature, the permeation constant and the permeation activation energy can be obtained from an Arrhenius plot, see as an example Fig. 1. If the data does not fulfill the Arrhenius equation, a second temperature (points cannot be fitted with a line) or pressure dependence (lines of different pressures are not parallel to each other) of the permeation process is indicated. Furthermore, from the pressure dependence the limiting regime can be derived. In the diffusion-limited case, the permeation flux is proportional to the square root of the pressure, see Eq. 1. If the surface processes are limiting the permeation flux, the flux is proportional to the pressure [5,6]. Therefore, the slope of the pressure dependence yields the information on the limiting regime.

For the analysis of the lag-time, the increase of the permeation flux versus time is integrated, see Fig. 2b. The lag-time (L) is obtained from the abscissa value at $y = 0$ from a line fitted to the linear part of the graph [7]. The diffusion coefficient D of deuterium through the sample is calculated by $D = \frac{d^2}{6L}$. By measuring the lag-time at different temperatures and pressures, the diffusion constant D_0 and the diffusion activation energy E_D can be obtained from an Arrhenius plot $D = D_0 e^{\frac{-E_D}{RT}}$. Taking the values for P_0 and E_P into account, the solubility constant and the heat of dissolution can be calculated.

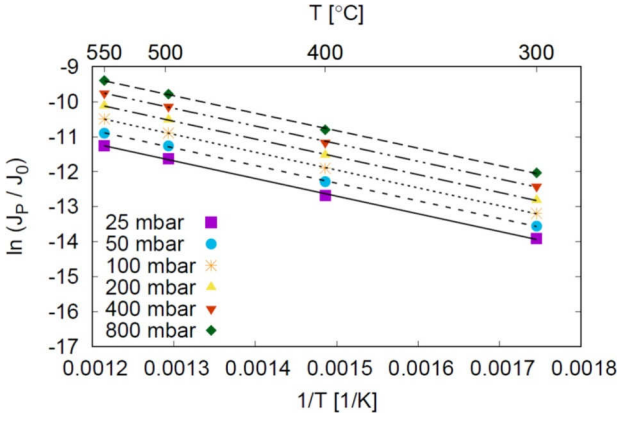

Fig. 1. Arrhenius plot for the sample Eu97 with $J_0 = 1\frac{\text{mol}}{\text{m}^2\text{s}}$. The lines represent the fitted lines to the data in order to obtain E_P and P_0, see Table 1. The color points represent the measurement points at different applied deuterium pressures.

Eu97	0.5	5.7(4)	41.6(5)	–			
316L	0.5	8(1)	58(1)	6(1)	51(1)	1(2)	7(2)
oxi_Eu97	0.55	5(2)	46(1)	–	–	–	–
rou_316L	0.6	7(1)	63(1)	1(1)	47(1)	7(2)	16(2)

4. Results

As described above, all samples were analyzed by SEM(FIB). No smear layer can be detected on both polished samples (Eu97 and 316L) with SEM in the cross section (FIB), see Fig. 3. Due to the oxidation procedure of the oxi_Eu97 sample, an about 30 nm thick continuous chromium oxide layer was produced at the surface and on top of this chromium oxide layer iron oxide particles with a size of about 80 nm are found in SEM(FIB) images, see Fig. 3d. The oxides were analyzed by EDX, not shown. The grinding procedure of the rou_316L sample leads to a scratch depth in the range of 500 nm, see Fig. 3e. On top of this surface profile an about 500 nm thick smear layer is observed in the same SEM(FIB) image. The smear layer is produced by stress introduced on the surface due to the grinding procedure and consists of the same material as the bulk sample. No oxygen was observed by EDX, not shown. The grain size is much smaller and the microstructure is different in the smear layer compared to the bulk of the sample.

The permeation flux versus the applied deuterium pressure is shown in Fig. 4. In all samples there is no difference in the permeation flux between the two measurements at a specific temperature (not shown), which confirms that there is no change of sample state (e.g. oxidation) during the measurement cycle. The slope (x) of the permeation flux versus temperature is indicated in Table 1. For all samples, the Arrhenius equation is fulfilled and the lines for different pressures are parallel to each other. As an example, the Arrhenius plot for the sample Eu97 is shown in Fig. 1. The obtained values for P_0 and E_P are shown in Table 1, as well.

The deuterium lag-time was measured for the 316L and rou_316L samples. The data for the 316L sample are shown in Fig. 2 as an example. The obtained values for D_0, E_D, K_0 and ΔH are shown in Table 1.

5. Discussion

The deuterium permeation through the two polished samples (Eu97 and 316L) is limited by diffusion ($J_P \sim p^{0.5}$), they are both in the diffusion-limited regime. The pressure dependence of the permeation flux through the oxi_Eu97 and the rou_316L sample shows a slight deviation from the square root pressure dependence. Therefore, one can assume that in these samples the surface processes have a small influence on the permeation process. Nevertheless, the major limiting process for the permeation flux is diffusion for all materials investigated in this work.

The permeation flux of Eu97 and 316L is in good agreement with the published data in Causey et al. [5] for RAFM steels (Eu97) and austenitic stainless steel (316L). The permeation flux through the Eu97 sample is about one order of magnitude higher than through the 316L sample. This can be explained by the huge difference in microstructure, see Fig. 3a and b. The grain size in the Eu97 sample is smaller by two orders of magnitude compared to the 316L sample. Furthermore, as a rule of thumb, there is a slower deuterium diffusion through fcc (316L)

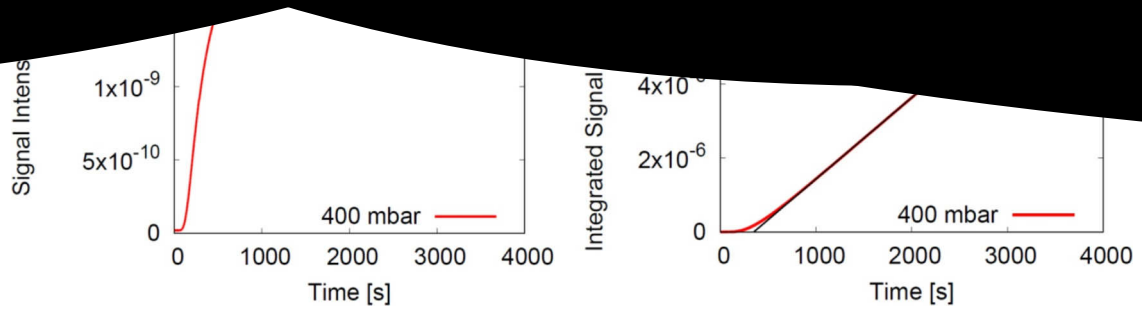

Fig. 2. a) Time-lag measurement (D_2 mass spectrometer signal versus time) on the sample 316L at 400°C and ***400*** mbar. b) Integrated intensity signal versus time from the data shown in a). The black line indicates the line fit to the linear part of the curve. The lag-time is defined as the abscissa value at $y = 0$, in this case 350 s.

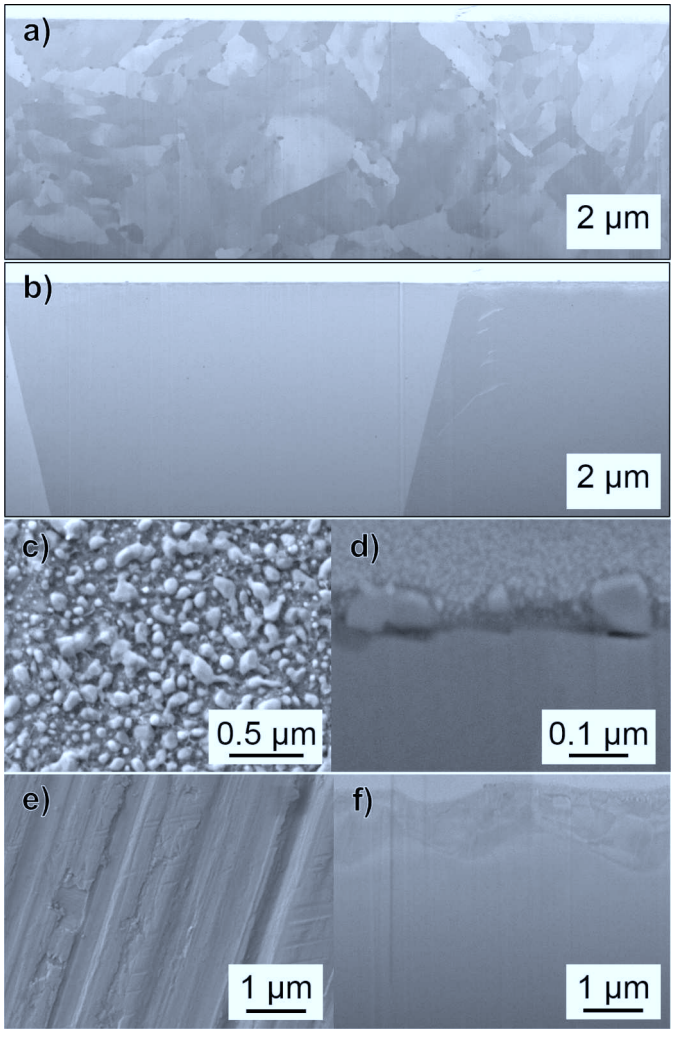

Fig. 3. a) SEM on a cross section prepared by FIB of the sample Eu97. The bright area at the top is a platinum layer, which was deposited in order to perform the FIB cut. b) SEM on a cross section of the sample 316L. The bright area at the top is a platinum layer. c) Top view SEM on the oxi_Eu97 sample. d) SEM on a cross section of the sample oxi_Eu97. The dark area on top of the Eu97 surface is a chromium oxide, the grains are iron oxide, as analyzed by EDX. The bright area at the top of the figure is a platinum layer. e) Top view SEM on the rou_316L sample. f) SEM on a cross section of the sample rou_316L. The smear layer of about 500 nm is visible. The bright area at the top is a platinum layer.

metals than through bcc (Eu97) metals [8]. We did not measure the same lattice structure with different microstructure, which is not relevant in steels, since steels are not only defined by the composition but the microstructure as well. Nevertheless, we assume that the main deuterium diffusion is through the grain boundaries and not through the lattice. Due to this reason, the difference in microstructure is assumed to be the main reason for the lower deuterium permeation flux through 316L compared to Eu97.

By oxidizing the surface of the Eu97 sample, the permeation flux is lowered. The chromium/iron oxide layer reduces the permeation flux by less than an order of magnitude. The permeation constant remains at the same value and the permeation activation energy is slightly increased, if one compares the samples Eu97 and oxi_Eu97. A natural oxide layer on steel samples has a permeation reduction factor (J_P of the substrate divided by J_P of the oxidized or coated substrate) of less than an order of magnitude and is therefore not sufficient as permeation barrier. Depending on the reactor concept and place of application in the reactor, TPB have to be applied, which reduce the permeation flux by at least two orders of magnitude [2,3].

The roughening of the 316L substrate surface lowers the permeation flux as well. Due to the fact that the permeation through the 316L samples is diffusion-limited, the effect of the surface roughening is expected to be small [9]. The slight decrease of the permeation flux through the rou_316L sample compared to the 316L sample might therefore be caused by the smear layer on top of the roughness profile. The permeation constant is similar in both 316L samples, whereas the permeation activation energy is increased for the roughened surface. Comparing the diffusion of 316L and rou_316L, the diffusion constant and the diffusion activation energy are lower in rou_316L. This leads to a lower diffusion coefficient of rou_316L in the measured temperature regime. With the assumption that the diffusion coefficient of the bulk of the sample is not changed, the diffusion process in the smear layer is slower compared to the diffusion in the bulk of the sample. Furthermore, the solubility of the rou_316L sample is higher compared to the 316L sample. This leads to the conclusion that more deuterium will be stored in the smear layer compared to the bulk part of the sample. The different diffusion coefficient and solubility of the smear layer compared to the bulk can be explained by the different grain size and microstructure, see Fig. 3. There might be more traps and different grain boundaries in the smear layer, which have an influence on the permeation flux [10]. To conclude, we assume, that due to the smear layer, the permeation flux is slightly reduced in the rou_316L sample, the diffusion coefficient is lower and the solubility is higher at the measured temperature range. However, due to the uncertainties of the data and due to the reason that the sample is not in the diffusion-limited regime, one has to be careful with the interpretation and further measurements have to be done in order to clarify this behavior.

In order to provide an estimate for the permeation behavior of

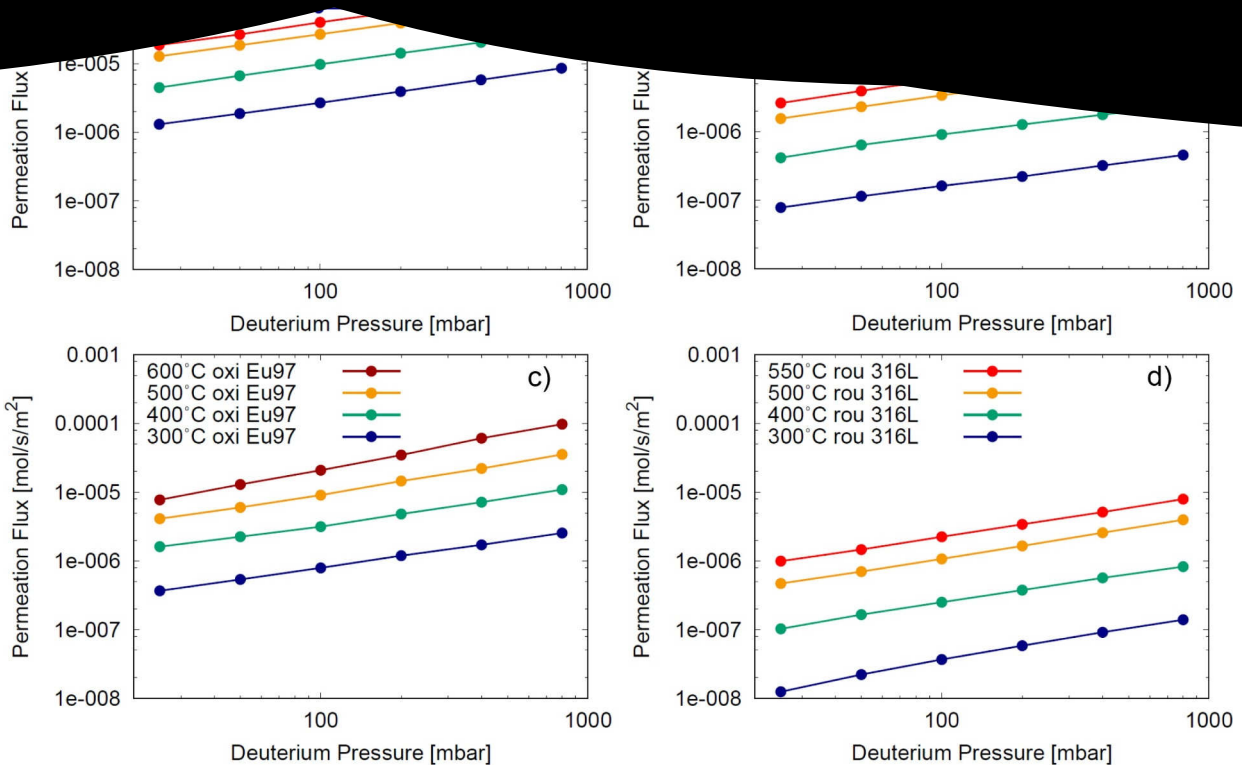

Fig. 4. The deuterium permeation flux versus the applied deuterium pressure through samples a) Eu97, b) 316L, c) oxi_Eu97, and d) rou_316L. The colors represent the sample temperature. Note that in case of the oxi_Eu97 sample the measurement was performed at 600°C instead of 550°C.

technical surfaces, one has to consider both effects of oxidation and roughening of the surface on the permeation flux. In both cases we observed a small reduction of the permeation flux. Therefore, we conclude that the permeation flux is reduced by maximum one order magnitude due to technical surfaces compared to polished surfaces. The reduction of the permeation flux due to surface roughening by plasma exposure is also less than one order of magnitude. In future fusion devices (e.g. DEMO) the deuterium permeation will not be sufficiently reduced by a technical surface and TPB have to be applied, which reduce the permeation flux by at least two orders of magnitude.

6. Conclusions

In both polished steels samples, Eu97 and 316L, the deuterium permeation flux is limited by diffusion. The permeation flux through the 316L sample is about one order of magnitude smaller than through the Eu97 sample and the permeation activation energy is higher. Oxidation or roughening of the surface leads to a small reduction of the permeation flux. It is supposed that in the case of roughening, the reduction is due to the lower diffusion coefficient and the higher solubility in the smear layer compared to the bulk. We conclude that a technical surface will reduce the deuterium permeation flux by less than one order of magnitude. In future fusion devices TPB are required for sufficient reduction.

Acknowledgments

The authors thank G. De Temmerman for providing the 316L(N)-IG sample material and B. Göths for sample preparation. This work has been carried out within the framework of the EUROfusion Consortium and has received funding from the Euratom research and training programme 2014–2018 and 2019–2020 under grant agreement no 633053. The views and opinions expressed herein do not necessarily reflect those of the European Commission.

References

[1] H. Nakamura, S. Sakurai, S. Suzuki, T. Hayashi, M. Enoeda, K. Tobita, Case study on tritium inventory in the fusion demo plant at jaeri, Fusion Eng. Des. 81 (8-14) (2006) 1339–1345, https://doi.org/10.1016/j.fusengdes.2005.10.009.

[2] F. Franza, Tritium Transport Analysis in HCPB DEMO Blanket With the FUS-TPC Code, Report-Nr. KIT-SR 7642, Karlsruhe Institute of Technology, 2013.

[3] D. Demange, L. Boccaccini, F. Franza, A. Santucci, S. Tosti, R. Wagner, Tritium management and anti-permeation strategies for three different breeding blanket options foreseen for the european power plant physics and technology demonstration reactor study, Fusion Eng. Des. 89 (7–8) (2014) 1219–1222, https://doi.org/10.1016/j.fusengdes.2014.04.028.

[4] J. Engels, A. Houben, M. Rasinski, C. Linsmeier, Hydrogen saturation and permeation barrier performance of yttrium oxide coatings, Fusion Eng. Des. 124 (2017) 1140–1143, https://doi.org/10.1016/j.fusengdes.2017.01.058.

[5] R. Causey, R. Karnesky, C.S. Marchi, 4.16 - tritium barriers and tritium diffusion in fusion reactors, in: R.J. Konings (Ed.), Comprehensive Nuclear Materials, Elsevier, Oxford, 2012, pp. 511–549, , https://doi.org/10.1016/B978-0-08-056033-5.00116-6.

[6] C. Linsmeier, M. Rieth, J. Aktaa, T. Chikada, A. Hoffmann, J. Hoffmann, A. Houben, H. Kurishita, X. Jin, M. Li, A. Litnovsky, S. Matsuo, A. von Mller, V. Nikolic, T. Palacios, R. Pippan, D. Qu, J. Reiser, J. Riesch, T. Shikama, R. Stieglitz, T. Weber, S. Wurster, J.-H. You, Z. Zhou, Development of advanced high heat flux and plasma-facing materials, Nucl. Fusion 57 (9) (2017) 092007.

[7] R.M. Barrer, Diffusion in and Through Solids, Cambridge, England: The University Press, 1941.

[8] H. Wipf, Hydrogen in Metals III, Springer-Verlag, Berlin Heidelberg, 1997.

[9] A. Pisarev, I. Tsvetkov, S. Yarko, T. Tanabe, Hydrogen permeation through membranes with rough surface, AIP Conf. Proc. 837 (1) (2006) 238–249, https://doi.org/10.1063/1.2213079.

[10] J. Engels, A. Houben, P. Hansen, M. Rasinski, C. Linsmeier, Influence of the grain structure of yttria thin films on the hydrogen isotope permeation, Int. J. Hydrog. Energy 43 (51) (2018) 22976–22985, https://doi.org/10.1016/j.ijhydene.2018.09.191.